

## **The Role of Adiabaticity in the Aerosol First Indirect Effect**

Byung-Gon Kim<sup>@\*</sup>, Mark A. Miller<sup>#</sup>, Stephen E. Schwartz<sup>#</sup>,  
Yangang Liu<sup>#</sup>, Qilong Min<sup>§</sup>

<sup>@</sup>Department of Atmospheric Environmental Sciences,  
Kangnung National University, Gangnung, 210-702, Korea

<sup>#</sup>Environmental Sciences Department,  
Brookhaven National Laboratory, Upton, NY 11973 United States

<sup>§</sup>Atmospheric Science Research Center, State University of New York at Albany,  
251 Fuller Road, Albany NY, 12203, United States

All authors listed on the manuscript concur with submission in its revised form.

Revised on October 29, 2007

**accepted JGR Atmospheres 2007-11-07**

\* Corresponding Author: Byung-Gon Kim  
123, Jibyundong, Gangnung, 210-702  
Department of Atmospheric Environmental Sciences  
Kangnung National University, Korea  
Email) [bgk@kangnung.ac.kr](mailto:bgk@kangnung.ac.kr)  
Tel) 82-33-640-2326  
Fax) 82-33-640-2320

## The Role of Adiabaticity in the Aerosol First Indirect Effect

Byung-Gon Kim<sup>@</sup>, Mark A. Miller<sup>#</sup>, Stephen E. Schwartz<sup>#</sup>,  
Yangang Liu<sup>#</sup>, Qilong Min<sup>§</sup>

<sup>@</sup>Department of Atmospheric Environmental Sciences,  
Kangnung National University, Gangnung, 210-702, Korea

<sup>#</sup>Environmental Sciences Department,  
Brookhaven National Laboratory, Upton, NY 11973 United States

<sup>§</sup>Atmospheric Science Research Center, State University of New York at Albany,  
251 Fuller Road, Albany NY, 12203, United States

### Abstract

Aerosol indirect effects are the most uncertain of the climate forcing mechanisms that have operated through the industrial period. Several studies have demonstrated modifications of cloud properties due to aerosols and corresponding changes in shortwave and longwave radiative fluxes under specific cloud conditions, but some recent studies have indicated that cloud dynamical processes such as entrainment-mixing may be the primary modulator of cloud optical properties in certain situations. For example, day-to-day variations of the cloud drop effective radius ( $r_e$ ) determined from the ground-based remote sensing at the Southern Great Plains were found to be weakly associated with the variations in aerosol loading as characterized by its light-scattering coefficient at the surface, implying that other processes were impacting the cloud radiative properties. To study these other impacts, we extend a previous study to investigate the role of changes in liquid water path (LWP) and  $r_e$  in single layer stratiform clouds that are induced by entrainment-mixing processes and their effects on cloud radiative properties. We quantify the degree of entrainment-mixing in terms of the adiabaticity defined as the ratio of the observed cloud liquid water path to the corresponding adiabatic value. The cloud optical depth is, as expected, governed primarily by LWP, but that adiabaticity is the next most influential factor. In contrast,  $r_e$  is found to be equally sensitive to adiabaticity and LWP. In adiabatic clouds the aerosol first indirect effect is clearly observed and related to independent measures of aerosol loading. In sub-adiabatic clouds the aerosol first indirect effect is not readily observed; this may in some circumstances be

due to interference from heterogeneous mixing processes that change the droplet number density in a manner that attenuates the effect.

Keywords: aerosol, adiabaticity, effective radius, liquid water path

## **1. Introduction**

Clouds are an important regulator of the earth's radiation budget. Measurements of the Earth Radiation Budget Experiment [Collins et al., 1994] indicate that small changes in the macrophysical and microphysical properties of clouds have significant effects on climate, and a 5% increase in shortwave cloud forcing would compensate the increase in greenhouse gases between the years 1750 – 2000 [Ramaswamy et al., 2001]. Meanwhile, substantially increasing aerosols during the industrial period may have affected global climate by altering cloud microphysical and radiative properties, so-called the aerosol indirect radiative forcing, which remains one of the largest uncertainties in climate modeling and climate change prediction [IPCC, 2007; see Figure SPM-2]. The root of this uncertainty is a lack of fundamental understanding of the feedbacks of external forcings on clouds and adequate parameterizations of important processes [Lohmann and Feichter, 2005; Lohmann et al., 2007].

Increases in anthropogenic sources of cloud condensation nuclei (CCN) may increase cloud albedo by increasing the concentration and reducing the size of cloud droplets, in the absence of other mitigating factors [Twomey, 1977; the aerosol first indirect effect], which has strong observational support [Han et al., 1998; Brenguier et al., 2000; Nakajima et al., 2001; Schwartz et al., 2002; Kim et al., 2003; Feingold et al., 2003; 2006]. Additionally, a reduction in the size of cloud droplets could suppress precipitation and result in increased cloud lifetimes (aerosol second indirect effect) [Albrecht, 1989], which has been supported by limited observations [Rosenfeld, 2000; Kaufman et al., 2005; Rosenfeld et al., 2006]. While these mechanisms apply uniformly to the cloud droplet size distribution and uniformly reduce droplet size, recent studies have shown that an increase in aerosol loading leads to an increase in the relative dispersion of the size distribution of cloud droplets as well, and the enhanced dispersion (dispersion effect) acts

to diminish the cooling effect associated with the aerosol first indirect effect [Liu and Daum, 2002; Rotstayn and Liu, 2003; Peng and Lohmann, 2003]. The dispersion effect has been further confirmed by subsequent theoretical studies [Liu et al., 2006], parcel model simulations [Yum and Hudson, 2005; Peng et al. 2007], and field campaigns [Lu et al., 2007; Daum et al., 2007].

Several observational strategies have been used to study aerosol indirect effects. One approach combines remote sensing of cloud radiative properties with in-situ characterization of cloud microphysics during intensive, but short-lived, field campaigns [Radke et al., 1989; Brenguier et al., 2000]. An alternative approach uses satellite remote sensing to systematically characterize the aerosol effects on global basis, albeit with a limited spatial resolution [Han et al., 1998; Nakajima et al., 2001; Breon et al., 2002]. Yet another approach uses long-term measurements obtained with ground-based remote sensors to examine the relation of aerosols with cloud microphysics at specific sites [Feingold et al., 2003; Kim et al., 2003; Garrett et al., 2004].

In previous work [Kim et al., 2003], we have found in measurements in north central Oklahoma that the cloud drop effective radius ( $r_e$ ) in persistent single-layer stratiform clouds on different days was weakly associated with the variation in aerosol loading characterized by its light-scattering coefficient at the surface; this association is supportive of the aerosol first indirect effect, but there was substantial scatter in the observations, which was attributed to unquantified meteorological influences such as drizzle and entrainment. These processes lead to the subadiabatic liquid water content profiles frequently observed in the continental and marine stratus clouds [Kim et al., 2005; Chin et al., 2000; Miller et al., 1998; Albrecht et al., 1990]. Other factors that may have contributed to this scatter involve in the cloud droplet nucleation process, which is dependent on aerosol characteristics (chemical composition and size distribution etc) [Nenes et al., 2002; Chuang et al., 2002; Breon et al., 2002] and the updraft velocity; the latter implies a link to static stability [Feingold et al., 1999; Kim et al., 2003; Leaitch et al., 1996]. Recently Shao and Liu [2006] demonstrated the strength of the aerosol first indirect effect is about half that estimated by many previous investigators, and attributed the difference to the evaporation associated with entrainment-mixing processes. Especially the LWP is known to play a major role in determining the clouds' radiative

forcing [Dong et al., 2002; Kim et al., 2005]. The variation of LWP due to these non-adiabatic processes would induce the uncertainty in estimating aerosol indirect effect.

Ideally, all the controlling factors described above should be considered in order to better understand aerosol indirect effect. The problem is that these mechanisms appear to be dependent upon each other, and accounting for them is impossible with the current understanding of aerosol indirect effect. Therefore in the present study, the subadiabatic character of the clouds, or adiabaticity, is used to characterize the entrainment-mixing processes, and attempts are made to determine the extent to which these properties affect cloud optical properties, apart from the aerosol first indirect effect. For this purpose, we extend the previous one-year study to include 3-years (1999 ~ 2001) of data collected in relatively uniform stratus clouds by ground-based remote sensing at the Department of Energy Atmospheric Radiation Measurement (ARM) Southern Great Plain (SGP) site in north central Oklahoma.

This study is comprised of a section that details the data and analysis methods followed by a section that develops an analytical analysis of the relationship between adiabaticity and cloud optical properties under assumption that the clouds are homogeneously mixed. We apply this analytical formalism to data from the ground-based remote sensors with the goal of separating aerosol influences on cloud microphysics from meteorological factors and other cloud dynamics. Finally, we extend the analytical treatment to encompass the details of the mixing process in an effort to explain some of the features of the observed clouds.

## **2. Data and Methods**

The methods and data are similar to those used in Kim et al. [2003], except that the analysis period is extended by two years to encompass the period from 1999 to 2001. The primary instruments used in this study at the SGP site (97.48°W, 36.61°N) are in Table 1.

Cloud boundaries are retrieved every 10 seconds from a combination of data from active remote sensors, mainly a Millimeter-Wave Cloud radar (35 GHz), a micro-pulse lidar, and a ceilometer [Clothiaux et al., 2000]. The height resolutions of radar, lidar, and

ceilometer are 45m, 30m, and 15m, respectively. Liquid water path (LWP) is determined by a microwave radiometer (MWR), which measures time series of column-integrated liquid water based on the microwave emissions of liquid water molecules mainly at 31.4 GHz (vertically pointing; field of view 4.5° half width). The root mean square accuracies for cloud LWP retrievals are about 20 g m<sup>-2</sup> for LWP below 200 g m<sup>-2</sup> and 10% for LWP above 200 g m<sup>-2</sup> [Liljegren et al., 2001].

Cloud optical depth ( $\tau_c$ ) is measured with a Multi-Filter Rotating Shadowband Radiometer (MFRSR) at 415 nm; use of this single MFRSR channel minimizes sensitivity to surface reflectance. Use of the MFRSR limits the analysis to completely overcast conditions because of the wide field-of-view of the instrument (cosine-weighted hemispheric sensor for an effective half width of 120°); however restricting measurements to full overcast also minimizes effects of photon diffusion in clouds. Min and Harrison [1996] and Min et al. [2001] have developed a family of inversion methods to infer cloud optical properties from MFRSR and MWR. The cloud radiative properties are parameterized in terms of a cloud-average drop effective radius  $r_e$ , and total liquid water path, based on Mie theory [Hu et al., 1993]. In view of the dependence of Mie scattering properties on cloud drop radius, the effective radius is retrieved by an iterative procedure [Min and Harrison, 1996] that accounts for the variation of extinction efficiency with  $r_e$ . A sensitivity study illustrates that a 13% uncertainty in observed liquid water path (LWP, 20 g m<sup>-2</sup>) results in 1.5% difference in retrieved cloud optical depth and 12.7% difference in inferred cloud effective radius, on average [Min et al, 2003]. The uncertainty of the LWP measured by the microwave radiometer (MWR) is the major contributor to the uncertainty of retrieved cloud effective radius. In terms of remote sensing, however, the derivative of  $r_e$  is independent of LWP.

In the end, five-minute averaged  $\tau_c$ , LWP, and  $r_e$  values are used to characterize the cloud properties, which permits the narrow field of view measurement of LWP to be more compatible with the wide field of view measurement of  $\tau_c$  by the MFRSR, thereby ameliorating field-of-view issues.

Implicit in this measurement approach is the requirement that the clouds approximate a plane-parallel geometry. Hence, we restrict our examination to widespread,

low-level, non-precipitating, single-layer liquid water clouds without interference from higher-level clouds. Because we attempt to relate properties of aerosols measured at the surface with those influencing the properties of the cloud, we restrict cloud top height to be a maximum of 2-km above the ground. We also limit our analysis to well-mixed conditions, which are most likely to couple aerosol at the surface to that influencing the cloud [Feingold et al., 2006].

Because measurements of cloud condensation nuclei (CCN), which represent the fraction of all aerosols that may nucleate cloud droplets, were not available, measurements of light scattering coefficient of accumulation-mode aerosols with the aerodynamic diameter of 0.1 to 1.0  $\mu\text{m}$  by integrating nephelometers [Sheridan et al., 2001] are used as a CCN proxy for examination of aerosol influence. The use of light scattering coefficient as a proxy is generally defensible because the fraction of the total aerosol load that serves as CCN is typically found to be a relatively constant fraction of the total aerosol load, which is measured by the integrating nephelometers. Two nephelometers (TSI Model 3563), one dry and one humidified, measure the aerosol light scattering coefficient,  $\sigma_{sp}$ , as a function of relative humidity (RH) at three visible wavelengths (nominally 450, 550, and 700 nm). We use measurements at the 550 nm wavelength and low  $\text{RH} \leq 40\%$  to represent the light scattering coefficient of the dry aerosol. The TSI nephelometers are preceded by two impactors whose size cut switches every 6 minute; a 10- $\mu\text{m}$  impactor removes particles with aerodynamic diameter larger than 10  $\mu\text{m}$  and a 1- $\mu\text{m}$  impactor removes super micron size particles. In this study, we used scattering coefficient of accumulation-mode aerosols only, and thus measurements at 550-nm are available as 1-minute averages for five 6-minute intervals per hour, which are finally interpolated to 5-minute averages for comparisons with the cloud drop effective radius.

### **3. Effects of Cloud Adiabaticity**

#### **3.1. Adiabaticity and the Theoretical Derivation**

The propensity of layer clouds to maintain sub-adiabatic integrated liquid water path ( $W$ ) [Chin et al., 2000; Kim et al., 2005] motivates us to determine analytically the probable impacts of a reduction of liquid water on the cloud optical properties, relative to purely adiabatic clouds that are permitted no mixing or drizzle. In order to examine the effect of entrainment-mixing processes on cloud optical properties, we define the adiabaticity,  $\alpha$ , as

$$\alpha = \frac{W}{W_a}. \quad (1)$$

where the subscript “a” in  $W$  is referred to the adiabatic value. In addition, to isolate the impacts of entrainment mixing using  $\alpha$  as a proxy, we exclude any instances of the following significant drizzle; cloud reflectivity measured by the 35-GHz cloud radar was greater than  $-15$  dBz or the cloud base measured by this radar was lower than the optical cloud base, as measured by a laser ceilometer, which indicates drizzle in the subcloud layer [Kim et al., 2005]. The adiabatic LWP ( $W_a$ ) can be defined within the model of an adiabatic cloud for which LWC ( $L$ ) increases linearly with height above the cloud base [Albrecht et al., 1990]. For an isolated cloudy parcel experiencing adiabatic ascent in a shallow layer  $W_a$  can be written [Albrecht et al., 1990 and Roger and Yau, 1989] as

$$W_a = \frac{\bar{\rho}}{2} \bar{\Gamma}_l \Delta z^2 \quad (2)$$

$$\bar{\Gamma}_l = \frac{(\varepsilon + q_s) q_s l_v}{R_d T^2} \Gamma_w - \frac{g w_s p}{(p - e_s) R_d T} \quad (3)$$

$$\Gamma_w = -\frac{dT}{dz} = \Gamma_d \left( \frac{1 + l_v / R_d T}{1 + l_v^2 \varepsilon w_s / R_d C_p T^2} \right) \quad (4)$$

where  $\Gamma_l = dw_l/dz$  is the vertical variation of the adiabatic liquid water mixing ratio,  $w_l$ ;  $\bar{\rho}$  is the average air density,  $\varepsilon=0.622$ ,  $C_p$  is the specific heat content at constant pressure,  $q_s$  is the saturation mixing ratio of water vapor, and  $\Delta z$  is the cloud physical thickness,

$l_v$  is the latent heat of vaporization,  $R_d$  is the specific gas constant for dry air,  $e_s$  is the saturation vapor pressure,  $w_s$  is saturation mixing ratio of water vapor, and,  $\Gamma_d$  and  $\Gamma_w$  are the dry and moist adiabatic lapse rate, respectively.  $\Gamma_l$  is calculated using the mean temperature  $T$  and pressure  $P$  at the level of the cloud from the available soundings. Hence,  $W_a$  can be determined from the vertical profiles of thermodynamic structures and cloud thickness.

Considering a cloud of depth  $\Delta z$  and combining (1) and (2) yields

$$W = \alpha W_a = \frac{1}{2} \bar{\rho} \alpha \bar{\Gamma}_l \Delta z^2. \quad (5)$$

and substitution of (5) into the definition of effective radius of cloud droplets [Hansen and Travis, 1974] yields

$$\bar{r}_e = \frac{3}{4} \frac{\bar{\rho}}{\rho_l} \frac{\bar{\Gamma}_l \alpha \Delta z^2}{\tau_c}. \quad (6)$$

where  $\rho_l$  is the average liquid water density.

The effective radius, which is a key property of a cloud in characterizing the optical properties of the cloud [Hansen and Travis, 1974], can thus be retrieved by ground based remote sensors within the underlying assumptions that the radiation extinction efficiency,  $Q_e(r, z) \sim 2$  (large particle extinction limit) and that the scattering is conservative. The over bar indicates that  $r_e$  is a vertically integrated quantity for the entire cloud. Since  $W$  can be measured with a multi-channel MWR and  $\tau_c$  with a MFRSR,  $\bar{r}_e$  can be accordingly derived during the daytime in single layer liquid clouds.

Introducing  $N_{cd}$ , the number concentration of cloud drops at a given height within a cloud  $z$ ,  $N_{cd}(z) = \int n(r, z) dr$ , we note that if  $N_{cd}(z)$  is a constant independent of  $z$ ,  $N_{cd}(z) \approx N_{cd}$ , then  $\tau_c = 2\pi N_{cd} \iint r^2 dr dz$ , so information about the cloud droplet spectrum is required to proceed.

In order to represent this spectrum, we assume that the cloud drop size distribution can be represented by the  $k$ -th moment of a lognormal distribution given by  $\langle r^k \rangle = r_m^k \exp\left(k^2 \bar{\sigma}_r^2 / 2\right)$ , where  $k$  is the desired moment, and  $\bar{\sigma}_r$  is a measure of the relative dispersion of cloud droplet size distribution, the standard deviation of the logarithm of  $r$ , which is assumed to be constant for simplicity in this study. With these substitutions, the cloud optical depth is given by

$$\tau_c \cong 2\pi N_{cd} \bar{r}_m^2 \exp(2\bar{\sigma}_r^2) \Delta z, \quad (7)$$

where  $\bar{r}_m$  is the mean of droplet mode radius. Combining the LWP ( $W$ ) expressed in terms of the third moment of the cloud droplet size distribution and a moment generation function of  $\bar{r}_m$  leads to

$$W = \frac{4\pi}{3} \rho_l \bar{r}_m^3 N_{cd} \exp\left(\frac{9}{2} \bar{\sigma}_r^2\right) \Delta z, \quad (8)$$

and equating (5) and (8), and solving for  $\bar{r}_m$ , yields

$$\bar{r}_m = \left[ \frac{3}{8\pi} \frac{\bar{\rho}}{\rho_l} \frac{\bar{\Gamma}_l \alpha \Delta z}{N_{cd} \exp(9\bar{\sigma}_r^2/2)} \right]^{1/3}. \quad (9)$$

Substituting this expression into (7) produces

$$\tau_c = 2\pi \left( \frac{3}{8\pi} \frac{\bar{\rho}}{\rho_l} \right)^{2/3} \left[ \frac{\bar{\Gamma}_l^2 N_{cd} \alpha^2 \Delta z^5}{\exp(3\bar{\sigma}_r^2)} \right]^{1/3} \quad (10)$$

and upon substitution into (6) we obtain

$$\bar{r}_e = \exp(\bar{\sigma}_r^2) \left[ \frac{A\alpha\bar{\Gamma}_l\Delta z}{N_{cd}} \right]^{1/3} \quad (11)$$

where A is a constant, which is given by

$$A = \frac{3}{8\pi} \frac{\bar{\rho}}{\rho_l}. \quad (12)$$

The above derivation is based on assumption of the homogeneous mixing in that cloud properties through the entire cloud are assumed to be uniformly impacted by the reduction in liquid water path denoted by  $\alpha$ . As we will note later, this assumption has important implications in the interpretation of the observations.

Examination of the ARM data archive for three years (1999 - 2001) yielded fourteen analysis days (see Figure 4) for which the screening criteria were satisfied for 2 hours or more such that the cloud should be widespread, low-level, non-precipitating, single-layer liquid water only without interference from higher-level clouds and also located below 2-km above the ground with the well-mixed condition. Comparisons of the observed LWP with the adiabatic LWP are made for the 6 cases during which there were vertical soundings that permit the calculation of  $W_a$  by (2). Comparisons (Figure 1) reveal that most of the cases were subadiabatic except for 1999/03/23, which was nearly adiabatic. The subadiabatic cases have  $W/W_a$  ranging from 0.34 to 0.51; these values are somewhat lower than the mixing parameter ( $\alpha=0.6 \sim 0.7$ ) used by Boers and Mitchell [1994] in a maritime cloud system. The vertical variation of the adiabatic liquid water mixing ratio with height,  $\Gamma_l$ , ranged from 1.32 to 1.93 g kg<sup>-1</sup> km<sup>-1</sup> with an average value of 1.63 g kg<sup>-1</sup> km<sup>-1</sup>; this value is somewhat lower than that (2.10 g kg<sup>-1</sup> km<sup>-1</sup>) reported in marine boundary layer clouds off the Southern California coast [Albrecht et al., 1990].

### 3.2. Sensitivity of $r_e$ and $\tau_c$ to Adiabaticity

In order to investigate the dependence of  $r_e$  on  $\alpha$  (Figure 2a), we classify the data by cloud thickness with the separation of 200 – 1000 m into thin and thick cloud regimes by its mode value of 600 m. These data show an increase in  $r_e$  with an increase in  $\alpha$ , and segregation by cloud thickness. According to (11), if the mixing is homogenous we expect changes in  $r_e$  as a response to changes in  $\alpha$ ,  $\Delta z$ , or  $\sigma_r$ . Note that the relationship of  $r_e$  to  $\alpha$  is not as significant as that of  $r_e$  to  $\Delta z$  (Table 2). We cannot evaluate the relationship between  $r_e$  and  $\sigma_r$  because we have no means of directly measuring  $\sigma_r$ .

To quantify the sensitivity of (11), we take its logarithm and its derivative, which yields

$$\frac{\delta \bar{r}_e}{\bar{r}_e} = \delta \bar{\sigma}_r^2 + \frac{1}{3} \frac{\delta \alpha}{\alpha} + \frac{1}{3} \frac{\delta \Delta z}{\Delta z} - \frac{1}{3} \frac{\delta N_{cd}}{N_{cd}} \quad (13)$$

Equation (13) assumes a homogeneous mixing and a uniformly change of droplet size through the whole droplet spectrum. If we assume  $\bar{\sigma}_r$ ,  $\Delta z$ , and  $N_{cd}$  to be constant, a relative change in  $r_e$  is proportional to a relative change in  $\alpha$  with the slope of 1/3. The dashed reference line (Figure 2a) denotes  $r_e$  for  $N_{cd} = 288 \text{ cm}^{-3}$  and  $\bar{\sigma}_r = 0.35$ , values representing average values in continental clouds by Miles et al. [2000],  $\Gamma_l$  of  $1.63 \text{ g kg}^{-1} \text{ km}^{-1}$ , an average value obtained from 6 soundings of 14 candidates of this study, and the cloud thickness of 500m, which is the average cloud thickness. Neither the thick or thin cloud subgroups appear to possess the requisite 1/3 slope suggested by (11), though the thick clouds appear to more closely approximate the analytical formulation. We also note a lack of slope in the thin cloud regime, implying that  $r_e$  could be subject to variability in  $\bar{\sigma}_r^2$ .

We examine the dependence of  $r_e$  and  $\Delta z$  in more detail by classifying the data into different bins of  $\alpha$ : 0.1 – 0.8 (subadiabatic regime; blue dots in Figure 2b) and 0.8 – 1.2 (adiabatic regime; green dots in Figure 2b). A reference line denotes  $r_e$  for the same

conditions listed above, but for  $\alpha = 0.7$ . The sensitivity of  $r_e$  to  $\Delta z$  seems slightly stronger, as indicated by the closer proximity to the predicted 1/3 slope. The stronger association of  $r_e$  to  $\Delta z$  is shown in the adiabatic regime (slope = 0.42 and square of Pearson correlation coefficient  $R^2 = 0.48$ , in Table 2), which is comforting because  $r_e$  increases systematically in an adiabatic ascent. This relationship of  $r_e$  to  $\Delta z$  could be due to physical connections, since the  $r_e$  represents column averaged effective radius and the derivative of  $r_e$  is independent of LWP in terms of remote sensing. We conclude from this analysis that  $r_e$  is weakly associated with  $\alpha$ , a proxy for mixing and only dependent upon cloud thickness in spite of the assumption of constant droplet dispersion. The poor correlation of  $r_e$  with  $\alpha$  suggests that the homogeneous mixing is not the major mechanism of entrainment-mixing processes in these clouds.

The derivative of the cloud optical depth (10) can be expanded with the partial derivative of  $\alpha$ ,  $\Delta z$ , and  $N$  as,

$$\frac{\overline{\delta\tau_c}}{\tau_c} \propto \overline{\delta\sigma_r}^{-2} + \frac{1}{3} \frac{\delta N_{cd}}{N_{cd}} + \frac{2}{3} \frac{\delta\alpha}{\alpha} + \frac{5}{3} \frac{\delta\Delta z}{\Delta z}. \quad (14)$$

This equation specifies that the relative change in  $\Delta z$ , or equivalently LWP, is the major contributor to the relative change in  $\tau_c$ , which is also supported by the observations from the ground-based remote sensors (Figure 3). Here the reference line denotes the same conditions listed above, but with  $\Delta z = 500m$  rather than a fixed value of  $\alpha$ . There is a notable increase in  $\tau_c$  with an increase in  $\alpha$  and distinct segregation in the two cloud thickness populations, characteristics that are predicted by (10).

We plotted  $\tau_c$  against  $\Delta z$  to evaluate the sensitivity of  $\tau_c$  to changes in  $\Delta z$  for different values of  $\alpha$  (Figure 3b). The sensitivity of  $\tau_c$  to  $\Delta z$  is greater than that of  $\tau_c$  to  $\alpha$ , as seen by noting the similarity in the slopes for different  $\alpha$  bins. Similar to Figure 2 where we found that  $r_e$  was more significantly correlated with  $\Delta z$  than with  $\alpha$ , we also find the most significant correlation between  $\tau_c$  and  $\Delta z$ . Note that the sensitivity of  $\tau_c$

to  $\Delta z$  and  $\alpha$  is 5 fold and 2 fold greater, respectively, than that of  $r_e$  to  $\Delta z$  and  $\alpha$  (Equations 13 and 14; Table 3).

This formula and supportive observations illustrate the potential linkages with various physical parameters and especially the strong dependence of cloud optical depth upon cloud thickness, or equivalently, LWP. In addition, the derived formula showed that adiabaticity effect has twice that of the cloud droplet number concentration in modulating increases in the cloud optical depth, and, as a consequence, the albedo with the assumption of a homogeneous mixing and a uniform change of droplet size. The observation strongly suggests that mixing processes may overwhelm the reduction in cloud droplet size dictated by the nucleation processes that underlie the theory of the aerosol first indirect effect.

#### **4. Aerosol First Indirect Effects and Adiabaticity**

The observed cloud optical properties ( $r_e$  and  $\tau_c$ ) were related to the cloud structural parameters  $\alpha$ , a proxy for the entrainment-mixing process, and  $\Delta z$ , a proxy for LWP in the previous section. In this section, we examine the relationship between  $r_e$  and aerosol loading, thereby enabling us to evaluate the extent to which aerosols are changing  $r_e$ , and whether its magnitude rivals that of the structural parameters examined above.

##### **4.1. Relationship of $r_e$ to Aerosol Load**

The aerosol light scattering coefficient  $\sigma_{sp}$  has been used as a proxy for the aerosol loading, and ultimately, the CCN concentration in the previous studies [Kim et al., 2003; Garrett et al., 2004]. The mixing state of the boundary layer must be considered to insure that the surface aerosol observations are representative of those that are influencing the cloud droplet nucleation properties of the clouds. Feingold et al. [2006] suggested that the optimal period for the use of this proxy is in daytime well-mixed cases, which we use here.

The aerosol indirect effect ( $IE$ ) has been defined as the derivative of the logarithm of cloud droplet radius with respect to the logarithm of the aerosol light scattering [Feingold et al, 2003];

$$IE = -d \log r_e / d \log \sigma_{sp} \quad (15)$$

Strictly speaking, the  $IE$  must be defined in terms of  $\tau_c$  rather than  $r_e$ , but (15) focuses on the reduction in droplet size and assumes that CCN have no impact on LWP. While there is scant evidence to support the dependence in LWP on CCN, dependence cannot be summarily dismissed in certain cloud conditions. The  $IE$  value emphasizes relative rather than absolute sensitivities, which is useful in reproducing trends without regard to the measurement biases [Garrett et al., 2004; Feingold et al., 2006]. It should be noted that the true manifestation of the aerosol first indirect effect rests upon the nucleation of observed aerosols into cloud droplets, which is better described by the CCN activity spectrum. In lieu of this measurement, Equation (15) not only assumes that there is a relationship between  $\sigma_{sp}$  and CCN, but that the updraft conditions that exist in cloud nucleate a constant fraction of CCN. While this condition cannot be insured in the current analysis, it is expected that many of the observed cases occur in similar conditions.

The relationships between  $r_e$  and  $\sigma_{sp}$  in the logarithm scale are shown in Figure 4 which indicates a general decrease in  $r_e$  with the increase of  $\sigma_{sp}$ , which, as expected, is consistent with Kim et al [2003] since the data used in the original analysis are a subset of those presented here. For the data set as a whole the value of  $IE$  is 0.15 ( $R^2 = 0.28$ ) (Figure 4a), which is a slightly better correlation than 0.13 ( $R^2 = 0.24$ ), which was found in Kim et al. [2003].

The physics that underlie the first indirect effect dictate that the  $IE$  comparison must be made between clouds having the same liquid water content because  $r_e$  is also a function of LWP [Twomey, 1991; Garrett et al., 2004; Feingold et al., 2006]. Accordingly, the data are divided into 5 bins of LWP = 10-50, 50-100, 100-150, 150-200, and >200 g m<sup>-2</sup>, respectively. Values of  $IE$  range from 0.04 ~ 0.17 (Figure 4b and Table

4), indicating a decrease in  $IE$  with an increase in LWP and better correlation with the lower LWP, though the correlations are, in general, poor ( $R^2=0.02\sim 0.17$ ). Despite the poor correlations, these values are also compatible with the previous works using ground-based remote sensors; 0.02 ~ 0.16 in Feingold et al. [2003], and 0.13 ~ 0.19 in Garrett et al. [2004].

The  $IE$  values and adiabaticity ( $\alpha$ ) with 5 bins of LWP are demonstrated in Figure 5, respectively. The  $IE$  has relatively larger value around 50 - 150  $\text{g m}^{-2}$  bins, which is also coincident with larger value of adiabaticity, except for the bin of LWP less than 50  $\text{g m}^{-2}$ , where the measurement confidence is lowest. It is interesting to note that the higher the LWP, the more subadiabatic clouds are with the lowest bin of LWP excluded. The thicker clouds of high LWP tend to contain subadiabatic LWP and lower  $IE$  values, partly due to larger interacting surface area for the entrainment-mixing processes, which could eventually damp aerosol first indirect effect with an increasing LWP. Observational evidence that thicker clouds tend to exhibit stronger entrainment-mixing has also been reported from in-situ aircraft measurements [e.g., You and Liu, 1995].

The correlations between  $r_e$  and  $\sigma_{sp}$  are, in general, poor, despite the more extensive data set considered here. A natural question to pose is the extent to which the influence of aerosol loading on  $r_e$  might be dependent on the cloud structural parameters. In other words, are their specific structural configurations that permit cloud-aerosol interactions to dominate?

## 4.2. Aerosols Indirect Effect with the Change of Adiabaticity

To compute the adiabaticity  $\alpha$ , the averaged value ( $1.63 \text{ g kg}^{-1} \text{ km}^{-1}$ ) of the adiabatic lapse rates ( $\Gamma_l$ ) of LWC obtained from the six soundings was applied in the 14 cases (Figure 6). The calculation of  $\alpha$  strongly depend on  $\Delta z$  because the adiabatic LWP is proportional to square of cloud thickness, and linear proportional to  $\Gamma_l$  as seen in (6). In addition, the observation indicated that the relative variation of  $\Delta z$  is from 200m to 1000m greater than  $\Gamma_l$  ranging from 1.3 to 1.9  $\text{g kg}^{-1} \text{ km}^{-1}$ . Accordingly, the sensitive of

the adiabatic LWP to  $\Delta z$  is more than 7 times larger than that to  $\Gamma_l$ . Therefore, the current method using the averaged value of  $\Gamma_l$  is thought to introduce very little uncertainty in calculating  $\alpha$ .

Similar to the LWP bins of section 4.1,  $\alpha$  of 0.1 to 1.2 is divided into 2 classes: a subadiabatic regime (0.1 – 0.8) and an adiabatic regime (0.8 – 1.2). The thick cloud cases (600 to 1000 m) are not shown here because they are all generally subadiabatic (95%) with  $\alpha$  ranging from 0.1 to 0.8 (Table 5) and data points are very few (the number of points is 3 only) for the adiabatic clouds. Therefore, the cloud thickness over which both adiabatic and subadiabatic clouds exist is 200 to 600m, but only 8% of these clouds were found to be adiabatic (Table 5). Poor correlations of  $r_e$  and  $\sigma_{sp}$  are indicated in the subadiabatic clouds and a negative slope (-0.17) with the significant correlation ( $R^2 = 0.53$ ) of  $r_e$  and  $\sigma_{sp}$  in the adiabatic cases. While the number of cases analyzed here is still small,  $r_e$  appears to have virtually no correlation with the  $\sigma_{sp}$  in the subadiabatic clouds associated with turbulent entrainment-mixing processes.

These results suggest that entrainment-mixing processes have substantial effects on the optical properties of these subadiabatic clouds which constitute a large fraction of the clouds that we observed. The predilection of the clouds at SGP to be subadiabatic due to entrainment-mixing could partly explain why it is hard to detect the aerosol indirect effect, as we will later demonstrate analytically. It is noteworthy that the reasons could partly be observational uncertainty [Kim et al., 2003] or an instrument collocation problem [Feingold et al., 2006] even though we tried to reduce these uncertainty and problem through the strict criteria and careful data screening processes.

Box plots of cloud optical properties (Figure 7; LWP,  $\tau_c$  and  $r_e$ ) for the subadiabatic and adiabatic clouds indicate consistently higher values of LWP and  $\tau_c$  for adiabatic clouds. Conversely,  $r_e$  shows no sensitivity to adiabaticity. Note that the notches represent a robust estimate of the uncertainty about the medians for box-to-box comparison. The boxes representing LWP and  $\tau_c$ , whose notches do not overlap, indicate that the medians of the subadiabatic cases differ from the adiabatic ones at the 5% significance level, whereas boxes of  $r_e$  overlap each other. The subadiabatic clouds

at the SGP site generally contain less cloud water, on the average, than they would have if they were adiabatic for the thin cloud with cloud thickness of 200 ~ 600 m, which is attributable to entrainment-mixing process. Accordingly the cloud optical depth, which is mostly a function of LWP, is understandably decreased when there is a reduction of LWP. Meanwhile, the cloud droplets effective radius could either increase or decrease, depending on homogeneous and heterogeneous mixing conditions, as explained in the following section 4.3, which would lead to no significant difference of  $r_e$  between the adiabatic and subadiabatic clouds.

### 4.3 Further Discussion on Entrainment-Mixing Effects

Our simple expression based on the homogeneous mixing assumption accounts only for the effect of entrainment-mixing process on the liquid water content ( $L$ ). The implied sensitivity of the clouds at the SGP to entrainment-mixing motivates us to analytically explore how the specific details of the entrainment-mixing process may impact the efficacy of the aerosol first indirect effect and our ability to observe it. Without loss of generality, sensitivity to any entrainment-mixing mechanisms can be illustrated by writing (11) as

$$r_e = \left( \frac{3}{4\pi\rho_l} \right)^{1/3} \beta \left( \frac{L}{N_{cd}} \right)^{1/3} \quad (16)$$

where  $\beta$  is a dimensionless parameter depending on the relative dispersion of the droplet spectrum [Liu and Daum, 2002]. For an adiabatic cloud, we have

$$r_{ea} = \left( \frac{3}{4\pi\rho_l} \right)^{1/3} \beta_a \left( \frac{L_a}{N_{cd,a}} \right)^{1/3} \quad (17)$$

where the subscript  $a$  denotes adiabatic conditions. The effects of mixing on  $L$ ,  $N_{cd}$ , and  $\beta$  may be represented as

$$\alpha_x = \frac{x}{x_a} \quad (18)$$

where  $x$  represents the variable that is being considered. Substitution of (18) into (16) yields

$$r_e = \alpha_\beta \left( \frac{\alpha_L}{\alpha_N} \right)^{1/3} r_{ea} \quad (19)$$

which relates adiabatic to non-adiabatic conditions. According to (19), the cloud optical properties may respond in several ways depending on the nature of the entrainment-mixing process. Four extremes are evident in (19):

- (i) Extreme homogeneous mixing occurs if the mixing time scale is much faster than the time scale of evaporation so that all droplets are exposed to the same relative humidity. In this case,  $\alpha_N = 1$ , because the mixing process does not change  $N_{cd}$ , but evaporation reduces droplet sizes. This is the case considered in (11) and in the analysis above. Taking logarithms produces  $\ln r_e = \ln(\alpha_\beta) + \ln r_{ea} + \frac{1}{3} \ln \alpha_L$ , which is the equation of the line displayed in Figures 2 and 3.
- (ii) Extreme inhomogeneous mixing dictates that all droplets are exposed to different relative humidity and a constant portion of droplets of all sizes are totally evaporated. In this case,  $\alpha_N = \alpha_L$ , and we can write  $r_e = \alpha_\beta r_{ea}$ , which implies that effective radius is basically independent of  $\alpha_L$ .
- (iii) Secondary activation is diagnosed when  $\alpha_N > \alpha_L$ , so  $c = \alpha_L / \alpha_N$  decreases with decreasing  $\alpha_L$ , or stronger mixing brings in more newly activated droplets. In this case,  $r_e = \alpha_\beta (c)^{1/3} r_{ea}$ , we expect a steeper slope in the decrease in  $r_e$  as the cloud becomes more subadiabatic ( $\alpha_L$  decreases).

(iv) Enhanced growth occurs when some cloud droplets grow at the expense of others.

In this situation,  $\alpha_N < \alpha_L$ , which implies that  $c$  increases with decreasing  $\alpha_L$ , so stronger mixing results in less but bigger droplets. The same mathematical relationship as in the above (iii) applies, but there is an increase in the effective radius with a decrease in  $\alpha_L$ .

The possibilities suggested by the above extremes as applied to (19) are summarized in Table 6, which suggests that the nature of the mixing process may either attenuate or amplify the aerosol indirect effect. Thus, when the observed clouds are sub-adiabatic, the details of the mixing process may be important in determining the radiative impact of the clouds and may, in some circumstances, be the controlling factor.

In summary, it is more likely that the aerosol first indirect effect will be observed in unabated form in adiabatic clouds because they are free of processes such as drizzle and entrainment that may alter the cloud droplet spectrum after the nucleation process occurs. Adiabatic clouds are the exception rather than the rule in real continental clouds and our results suggest that diabatic processes may possess many configurations, particularly when the mixing is heterogeneous.

## 5. Conclusions

The impacts of mixing on the optical properties of continental stratus clouds were examined in the context of the aerosol indirect effect using ground-based remote sensing at SGP for several cases that occurred in 1999 ~ 2001. Adiabaticity was used as a proxy for mixing processes. The results suggested, as expected, that there is a strong dependence of cloud optical depth upon cloud thickness, (a surrogate for LWP) as already emphasized in Kim et al., [2003]. The theoretical derivation showed that the impact of adiabaticity is twice that of the cloud number concentration in determining the cloud optical depth for clouds with the assumption of a homogeneous mixing and a uniform change of droplet size. The observed adiabaticity with the change of LWP illustrated that the thicker clouds of high LWP tend to contain subadiabatic LWP with accordingly lower  $\alpha$  values, corresponding to lower  $IE$ , which could eventually damp

aerosol first indirect effect with an increasing LWP. A stronger association ( $IE=-0.17$  and  $R^2=0.53$ ) between cloud droplet effective radius and aerosol light scattering coefficients, a proxy for aerosol concentration and size, was found in adiabatic clouds. Poor correlations between the two variables were indicated in the subadiabatic clouds that are observed most frequently at SGP and other continental locations.

We were able to observe characteristics consistent with the aerosol first indirect effect in adiabatic clouds, while being unable to detect these characteristics in subadiabatic clouds. This difference is likely due to processes other than the aerosol first indirect effect modulating cloud optical properties in subadiabatic clouds. While we recognize that potential limitations in our measurements, particularly in the subadiabatic cases, our selection criteria are significantly stringent that these limitations have been minimized. We also demonstrated analytically that the details of the mixing process might confound detection of the aerosol indirect effect in subadiabatic clouds because homogeneous and heterogeneous mixing apparently produces different microphysical responses.

This study is limited to a continental site where dynamic range of  $r_e$  is almost less than 10  $\mu\text{m}$ . Including the observation data of other remote sites should broaden this range and could improve our understanding of the various manifestations of mixing and its interplay with the aerosol first indirect effect. We note that information of the vertical profile of thermodynamic state is crucial in understanding the cloud microphysics in association with the aerosol indirect effect and that this study was hampered by the sparse frequency of vertical soundings rather than the selection of cloudy periods. Therefore, more frequent balloon-borne soundings or alternative strategies to measure the thermodynamic profile are needed to better understand the influence of adiabaticity and meteorology on cloud drop size, so that these impacts can be sorted from those that are true manifestations of the aerosol first indirect effect. Lastly the quantitative analysis of drizzle and entrainment effects on adiabaticity and its association with the aerosol indirect effect is recommended for future study.

## Acknowledgments

B.-G. Kim was supported by the Climate Environment System Research Center and partly by Korea Research Foundation Grant funded by Korea Government (MOEHRD, Basic Research Promotion Fund) (KRF-2005-03-C00175). Drs. M. A. Miller, S. A. Schwartz, and Y. Liu are funded by the US Department of Energy's Atmospheric Radiation Measurement Program.

## References

- Albrecht, B.A. (1989), Aerosols, cloud microphysics, and fractional cloudiness, *Science*, *245*, 1227-1230, 1989.
- Albrecht, B.A., C.W. Fairall, D.W. Thomson, and A.B. White (1990), Surface-based remote sensing of the observed and the adiabatic liquid water content of stratocumulus clouds, *Geophys. Res. Lett.*, *17*, 89-92.
- Boers, R. and R.M. Mitchell (1994). Absorption and feedback in stratocumulus clouds influence on cloud top albedo, *Tellus*, *46A*, 229-241.
- Brenguier, J.L., H. Pawlowska, L. Schuller, R. Preusker, J. Fischer, and Y. Fouquart (2000), Radiative properties of boundary layer clouds: Droplet effective radius versus number concentration, *J. Atmos. Sci.*, *57*, 803-821.
- Breon, F.-M., D. Tanre, and S. Generoso (2002), Aerosol effect on cloud droplet size monitored from satellite, *Science*, *295*, 834-838.
- Chess, R.D. et al. (1990), Intercomparison and interpretation of climate feedback processes in 19 atmospheric general circulation models, *J. Geophys. Res.*, *95*, 16601-16615.
- Chin, H.S., D.J. Rodriguez, R.T. Cederwell, C.C. Chuang, A.S. Grossman, and J. Yio (2000), A microphysical retrieval scheme for continental low-level stratiform clouds: impacts of the subadiabatic character on microphysical properties and radiation budgets, *Mon. Wea. Rev.*, *128*, 2511-2527.
- Chuang, C.C., J.E. Penner, J.M. Prospero, K.E. Grant, G.H. Rau, and K. Kawamoto (2002), Cloud susceptibility and the first aerosol indirect forcing: Sensitivity to black carbon and aerosol concentrations, *J. Geophys. Res.*, *107*, doi:10.1029/2000JD 000215.
- Clothiaux, E.E., T.P. Ackerman, G.G. Mace, K.P. Moran, R.T. Marchand, M.A. Miller, and B.E. Martner (2000), Objective determination of cloud heights and radar reflectivities using a combination of active remote sensors at the ARM CART sites, *J. Appl. Met.*, *39*, 645-665.

- Collins, W.D., W.C. Connant, and V. Ramanathan (1994), Earth radiation budget, clouds, and climate sensitivity, in: *The Chemistry of the Atmosphere: its Impact on Global Change*, edited by J.G. Calvert, pp. 207-215, Blackwell Scientific Publishers, Oxford, UK.
- Daum, P. H., Y. Liu, R.L. McGraw, Y.-N. Lee, J. Wang, G. Senum, M. Miller, and J.G. Hudson (2007), Microphysical properties of stratus/stratocumulus clouds during the 2005 Marine Stratus/Stratocumulus Experiment (MASE). *Revised to J. Geophys. Res.*
- Feingold, G., A.S. Frisch, B. Stevens, W.R. Cotton (1999), On the relationship among cloud turbulence, droplet formation and drizzle as viewed by Doppler radar, microwave radiometer and lidar, *J. Geophys. Res.*, *104*, 22195-22203.
- Feingold, G., W. Eberhard, D.E. Lane, and M. Previdi (2003), First measurements of the Twomey effect using ground-based remote sensors, *Geophys. Res. Lett.*, *1287*, doi:10.1029/2002GL016633.
- Feingold, G., R. Furrer, P. Pelewskie, L.A. Remer, Q. Min, and H. Jonsson (2006), Aerosol indirect effect studies at Southern Great Plains during the May 2003 intensive operation period, *J. Geophys. Res.*, *111*, doi10.1029/2004JD005648.
- Garrett T. J., C. Zhao, X. Dong, G. G. Mace, and P. V. Hobbs (2004) Effects of varying aerosol regimes on low-level Arctic stratus, *Geophys. Res. Lett.*, *31*, L17105, doi:10.1029/2004GL019928.
- Han, Q.Y., W.B. Rossow, J. Chou, and R. Welch (1998), Global surveys of the relationships of cloud albedo and liquid water path with droplet size using ISCCP, *J. Clim.*, *11*, 1516-1528.
- Hansen, J.E., and L.D. Travis (1974), Light scattering in planetary atmospheres, *Space Sci. Rev.*, *16*, 527-610.
- Hu, Y.X., and K. Stamnes (1993), An accurate parameterization of the radiative properties of water clouds suitable use of in climate clouds, *J. Clim.*, *6*, 728-742.
- International Panel on Climate Change (2007), *Climate Change 2007: The physical basis, Summary for Policymakers.*
- Kim, B.-G, S.E. Schwartz, M.A. Miller, and Q. Min (2003), Effective radius of cloud droplets by ground-based remote sensing: Relationship to aerosol, *J. Geophys. Res.*, *108*, doi:10.1029/2003JD003721.
- Kim, B.-G., S.A. Klein, and J.R. Norris (2005), Continental liquid water cloud variability and its parameterization using ARM data, *J. Geophys. Res.*, *110*, doi:10.1029/2004JD005122.
- Leitch, W.R., C.M. Banic, G.A. Isaac, M.D. Couture, P.S.K. Liu, I. Gultepe, S.-M. Li, L. Kleinman, P.H. Daum, and J.I. MacPherson (1996), Physical and chemical observations in marine stratus during the 1993 North Atlantic Regional Experiment: Factors controlling cloud

- droplet number concentrations, *J. Geophys. Res.*, *101*, 29123-29135.
- Liljegren, J.C., E.E. Clothiaux, G.G. Mace, S. Kato, and X. Dong (2001), A new retrieval for cloud liquid water path using a ground-based microwave radiometer and measurements of cloud temperature, *J. Geophys. Res.*, *106*, 14485-14500, 2001.
- Liu, Y. and P.H. Daum (2002), Indirect warming effect from dispersion forcing. *Nature*, *419*, 580-81.
- Liu, Y., P.H. Daum, and S.S. Yum (2006), Analytical expression for the relative dispersion of the cloud droplet size distribution, *Geophys. Res. Lett.*, *33*, doi:10.1029/2005GL024052.
- Lohmann, U. and J. Feichter (2005), Global aerosol indirect effects: a review, *Atmos. Chem. Phys.*, *5*, 715-737.
- Lohmann, U., P. Stier, C. Hoose, S. Ferrachat, S. Kloster, E. Roeckner, and J. Zhang (2007), Cloud microphysics and aerosol indirect effects in the global climate model ECHAM5-HAM, *Atmos. Chem. Phys.*, *7*, 3425-3446.
- Lu, M.-L., W.C. Conant, H. Jonsson, V. Varutbangkul, R.C. Flagan, and J.H. Seinfeld (2007), The Marine Stratus/Stratocumulus Experiment (MASE): Aerosol-cloud relationships in marine stratocumulus, *J. Geophys. Res.*, *112*, doi:10.1029/2006JD007985.
- Kaufman, Y.J., I. Koren, L.A. Remer, D. Rosenfeld, and Y. Rudich (2005), The effect of smoke, dust, and pollution aerosol on shallow cloud development over the Atlantic Ocean, *Proc. Natl. Acad. Sci.*, *102*, 11207-11212.
- Miles, N.L., J. Verlinde, and E. Clothiaux (2000), Cloud droplet size distributions in low-level stratiform clouds, *J. Atmos. Sci.*, *57*, 295-311.
- Min, Q., and L.C. Harrison (1996), An adjoint formulation of the radiative transfer method, *J. Geophys. Res.*, *101*, 1635-1640.
- Min, Q., L.C. Harison, and E. Clothiaux (2001), Joint statistics of photon path length and cloud optical depth: case studies, *J. Geophys. Res.*, *106*, 7375-7386.
- Min, Q.-L., M. Duan, and R. Marchand (2003), Validation of surface retrieved cloud optical properties with in situ measurements at the Atmospheric Radiation Measurement Program (ARM) South Great Plains site, *J. Geophys. Res.*, *108*, doi:10.1029/2003JD003385, 2003.
- Miller, M.A., M.P. Jensen, and E.E. Clothiaux (1998), Diurnal cloud and thermodynamic variations in the stratocumulus transition regime: A case study using in situ and remote sensors, *J. Atmos. Sci.*, *55*, 2294-2310.
- Nakajima, T., A. Higurashi, K. Kawamoto, and J.E. Penner (2001), A possible correlation between satellite-derived cloud and aerosol microphysical parameters, *Geophys. Res. Lett.*, *28*, 1171-1174.

- Nenes, A., R.J. Charlson, M.C. Facchini, M. Kulmala, A. Laaksonen, and J.H. Seinfeld (2002), Can chemical effects on cloud droplet number rival the first indirect effect?, *Geophys. Res. Lett.*, *29*, doi:10.1029/2002GL015295.
- Peng, Y., and U. Lohmann (2003), Sensitivity study of the spectral dispersion of the cloud droplet size distribution on the indirect aerosol effect, *Geophys. Res. Lett.*, *30*, doi:10.1029/2003GL017192.
- Peng, Y., U. Lohmann, R. Leaitch, and M. Kulmala (2007) An investigation into the aerosol dispersion effect through the activation process in marine stratus clouds, *J. Geophys. Res.*, *112*, doi:10.1029/2006JD007401.
- Radke, L.F., J.A. Coakley Jr., and M.D. King (1989), Direct and remote sensing observations of the effects of ships on clouds, *Science*, *246*, 1146-1149.
- Ramaswamy, V. et al. (2001), Radiative forcing of climate change, in: *Climate Change 2001: The Scientific Basis*. pp. 349-416, Cambridge Univ. Press, NY.
- Rogers, R.R. and M.K. Yau (1989), *A short course in cloud physics*, 293pp, Pergamon Press.
- Rosenfeld, D. (2000), Suppression of rain and snow by urban and industrial air pollution, *Science*, *287*, 1793-1796.
- Rosenfeld, D., Y.J. Kaufman, and I. Koren (2006), Switching cloud cover and dynamical regimes from open to closed Benard cells in response to the suppression of precipitation by aerosols, *Atmos. Chem. Phys.*, *6*, 2503-2511.
- Rotstajn L., and Y. Liu (2003), Sensitivity of the First Indirect Aerosol Effect to an Increase of Cloud Droplet Spectral Dispersion with Droplet Number Concentration, *J. Clim.*, *16*(21), 3476-3481.
- Schwartz, S.E., and C.M. Benkovitz (2002), Influence of anthropogenic aerosol on cloud optical depth and albedo shown by satellite measurements and chemical transport modeling, *Proc. Natl. Acad. Sci.*, *99*, 1784-1789.
- Shao, H., and G. Liu (2006) Influence of mixing on evaluation of the aerosol first indirect effect, *Geophys. Res. Lett.*, *33*, L14809, doi:10.1029/2006GL026021.
- Sheridan, P.J., D.J. Delene, and J.A. Ogren (2001), Four year of continuous surface aerosol measurements from the Department of Energy's Atmospheric Radiation Measurement program Southern Great Plains cloud and Radiation testbed site, *J. Geophys. Res.*, *106*, 20735-20747.
- Telford, J.W. (1996), Clouds with turbulence; the role of entrainment, *Atmos. Res.*, *40*, 261-282.
- Twomey, S. (1977), The influence of pollution on the shortwave albedo of clouds, *J. Atmos. Sci.*, *34*, 1149-1152.

- You, L., and Y. Liu (1995), Some microphysical properties of clouds and precipitation over China. *Atmos. Res.*, 35, 271-281.
- Yum, S.S., and J.G. Hudson (2005), Adiabatic predictions and observations of cloud droplet spectral broadness, *Atmos. Res.*, 73, 203-223.

## Figure captions

Figure 1. Comparisons of the observed LWP with the adiabatic LWP for the analysis period on 6 days. Blue line denotes the regression line of the observed vs. the adiabatic LWP.  $N$  denotes the number of data and  $m$  is the slope of the regression.

Figure 2. (a) Effective radii of cloud droplets as a function of  $\alpha$  with the different cloud height; the dot in blue color belongs to the thin cloud whose thickness ranges between 200 and 600m, whereas the dot in green color to the thick cloud between 600 and 1000m. Similarly (b)  $r_e$  as a function of the cloud thickness with the different adiabaticity; the blue dot belongs to subadiabatic cloud and the green dot to adiabatic cloud. The subadiabatic cloud denotes  $\alpha$  of 0.1 – 0.8 and the adiabatic cloud indicates  $\alpha$  of 0.8 – 1.2. The red dashed line of each figure indicates  $r_e$  for the indicated  $N$  of  $288 \text{ cm}^{-3}$ ,  $\Gamma_l$  of  $1.63 \text{ g kg}^{-1} \text{ km}^{-1}$ , and the cloud thickness of 500m and  $\alpha$  of 0.7, respectively.

Figure 3. The same as in Figure 2 except for cloud optical depth instead of  $r_e$ .

Figure 4. (a) Scatterplot of 5-min average  $r_e$  vs. light scattering coefficient ( $\sigma_{sp}$ ) for submicrometer aerosol at 550nm. Data for individual days are distinguished by color and symbol. (b) Scatterplot of  $r_e$  vs.  $\sigma_{sp}$  with the different LWP classes; The blue color indicates LWP of 10 - 50, the green 50 - 100, the red 100 – 150, the cyan 150 – 200, and the black larger than 200  $\text{g m}^{-2}$ . The slope of each solid line is a value of  $IE$ .

Figure 5.  $IE$  values (solid line) and adiabaticity (dotted line) according to the change of LWP.

Figure 6. Scatterplot of  $r_e$  vs.  $\sigma_{sp}$  for (a) the subadiabatic regime ( $0.1 < \alpha < 0.8$ ) and (b) the adiabatic regime ( $0.8 < \alpha < 1.2$ ) with the cloud thickness of 200 ~ 600m.

Figure 7. Box plots of LWP, cloud optical depth and  $r_e$  for the subadiabatic and adiabatic clouds for the thin cloud with cloud thickness of 200 ~ 600 m. The lower, middle and upper lines of the box are the 25<sup>th</sup>, 50<sup>th</sup> (median) and 75<sup>th</sup> percentiles of each variable, and an outlier is a value that is more than 1.5 times the interquartile range away from the top or bottom of the box. The notches represent a robust estimate of the uncertainty about the medians.

Table 1. Summary of primary instrumentation and value-added products<sup>a</sup>.

| Instrument  | Measured Quantities                                      | Comments  | Temporal resolution | References  |
|---|--|---|---------------------|---|
| MFRSR (Multi-Filter Rotating Shadowband Radiometer) | Cloud optical depth ( $\tau_c$ )                         | Measures direct and total-horizonal irradiances at 415 nm.                      | 20 s                | Min and Harrison (1996)   |
| MWR (Microwave Radiometer)                          | Liquid water path (LWP)                                  | Uses microwave brightness temperature,  | 20 s                | Liljegren et al. (2001)   |
| Nephelometer  | Scattering coefficient ( $\sigma_{sp}$ )                 | At 450, 550, 700 nm for the size of aerodynamic diameter less than 1 $\mu$ m    | 1 min               | Sheridan et al. (2001)<br><a href="http://www.cmdl.noaa.gov/aero/data/">http://www.cmdl.noaa.gov/aero/data/</a> . |
| ARSCL (Active Remotely-Sensed Cloud Locations)      | Cloud boundaries   | Best estimates from MMCR, Ceilometer and Lidar                                  | 10 s                | Clothiaux et al. (2000)   |
| BBSS (Balloon-Borne Sounding System)                | Temperature (T), Relative Humidity (RH), wind speed (WS) | Sounding at 6 hour intervals (3 hour interval for Intensive Observation Period) | 10 s                | <a href="http://www.arm.gov/docs/instruments/static/bbss.html">www.arm.gov/docs/instruments/static/bbss.html</a>  |

<sup>a</sup> Value-added products refer to data sets resulting from assimilation and analysis of data from multiple instruments.

Data are from [www.archive.arm.gov](http://www.archive.arm.gov) except where indicated.

Table 2. Summary of data numbers, the slope, and correlation coefficient of  $r_e$  vs.  $\alpha$  (upper) and  $r_e$  vs.  $\Delta z$  (lower) for each  $\Delta z$  bin and  $\alpha$  bin, respectively.

| Effective radius | $r_e$ vs. $\alpha$ |       | $r_e$ vs. $\Delta z$ |           |
|------------------|--------------------|-------|----------------------|-----------|
|                  | $\Delta z$ bins    |       | $\alpha$ bins        |           |
|                  | Thin               | Thick | subadiabatic         | adiabatic |
| N (data number)  | 216                | 58    | 232                  | 20        |
| Slope            | 0.07               | 0.21  | 0.21                 | 0.42      |
| $R^2$            | 0.07               | 0.16  | 0.11                 | 0.48      |

- The cloud thickness of 200 – 600 m belongs to the thin regime, and 600 – 1000m to thick regime.
- The subadiabatic cloud denotes  $\alpha$  of 0.1 – 0.8 and the adiabatic cloud indicates  $\alpha$  of 0.8 – 1.2.

Table 3. Summary of data numbers, the slope, and correlation coefficient of  $\tau_c$  vs.  $\alpha$  (upper) and  $\tau_c$  vs.  $\Delta z$  (lower) for each  $\Delta z$  bin and  $\alpha$  bin, respectively.

| Optical depth   | $\tau_c$ vs. $\alpha$ |       | $\tau_c$ vs. $\Delta z$ |           |
|-----------------|-----------------------|-------|-------------------------|-----------|
|                 | $\Delta z$ bins       |       | $\alpha$ bins           |           |
|                 | Thin                  | Thick | subadiabatic            | adiabatic |
| N (data number) | 216                   | 58    | 232                     | 20        |
| Slope           | 0.39                  | 0.30  | 0.98                    | 1.05      |
| $R^2$           | 0.29                  | 0.31  | 0.48                    | 0.67      |

- The cloud thickness of 200 – 600 m belongs to the thin regime, and 600 – 1000m to thick regime.
- The subadiabatic cloud denotes  $\alpha$  of 0.1 – 0.8 and the adiabatic cloud indicates  $\alpha$  of 0.8 – 1.2.

Table 4. Values of  $IE$ , correlation coefficient ( $R^2$ ), and data number (N) with the different classes of LWP.

| LWP<br>(g m <sup>-2</sup> ) | 10 ~ 50 | 50 ~ 100 | 100 ~ 150 | 150 ~ 200 | > 200 |
|-----------------------------|---------|----------|-----------|-----------|-------|
| $IE$ <sup>\$</sup>          | 0.17    | 0.09     | 0.10      | 0.08      | 0.04  |
| $R^2$                       | 0.17    | 0.12     | 0.15      | 0.08      | 0.02  |
| N                           | 92      | 126      | 155       | 44        | 77    |

<sup>\$</sup>  $IE$  is defined as  $-d \log r_e / d \log \sigma_{sp}$  and  $\sigma_{sp}$  indicates light scattering coefficient for submicron aerosol.

Table 5. Frequencies of the subadiabatic, adiabatic and superadiabatic clouds for each thin and thick cloud regime.

| Frequency | Thin Cloud regime |        |        | Thick Cloud regime |        |        |
|-----------|-------------------|--------|--------|--------------------|--------|--------|
|           | Sub.              | Adiab. | Super. | Sub.               | Adiab. | Super. |
| Number    | 177               | 17     | 22     | 55                 | 3      | 0      |
| (%)       | (82%)             | (8%)   | (10%)  | (95%)              | (5%)   |        |

- The cloud thickness of 200 – 600 m belongs to the thin regime, and 600 – 1000m to thick regime.
- The subadiabatic (Sub.) cloud denotes  $\alpha$  of 0.1 – 0.8, the adiabatic (Adiab.) cloud  $\alpha$  of 0.8 – 1.2, and the superadiabatic (Super.) cloud  $\alpha$  of 1.2 – 2.0.

Table 6. Potential response of cloud droplet effective radius to homogeneous and heterogeneous mixing processes.

|                           | Homogeneous Mixing                                      | Heterogeneous mixing/ETEM <sup>§</sup>       |  |  |
|---------------------------|---|--|--|--|
|                           |   | Extreme case                                 | Secondary activation   | Enhanced growth  |
| Underlying mechanism      | Faster Mixing   | Uniform evaporation                          | Nucleation   | Coalescence  |
| $\alpha_N$ and $\alpha_L$ | $\alpha_N=1$  | $\alpha_N = \alpha_L$                        | $\alpha_N > \alpha_L$  | $\alpha_N < \alpha_L$  |
| Mixing function           | Mixing does not change $N_{cd}$ but reduce the sizes    | Mixing changes $L$ & $N_{cd}$ proportionally | Stronger mixing results in more droplets,                                | Stronger mixing results in less but bigger droplets                      |
| Response of $r_e$         | Depending on $\alpha_\beta$ and $\alpha_L$              | $r_e$ independent of $\alpha_L$              | $r_e$ decreases with decreasing $\alpha_L$                               | $r_e$ increases with decreasing $\alpha_L$                               |
| Formula                   | $r_e = \alpha_\beta r_{ea} \left(\alpha_L\right)^{1/3}$ | $r_e = \alpha_\beta r_{ea}$                  | $r_e = \alpha_\beta \left(\frac{\alpha_L}{\alpha_N}\right)^{1/3} r_{ea}$ | $r_e = \alpha_\beta \left(\frac{\alpha_L}{\alpha_N}\right)^{1/3} r_{ea}$ |
| AIE Effect <sup>@</sup>   | Less AIE effect   | No change                                    | More AIE effect  | Less AIE effect  |

<sup>§</sup>ETEM means entity type entrainment mixing proposed by Telford (1995).

<sup>@</sup>AIE indicates aerosol indirect effect.

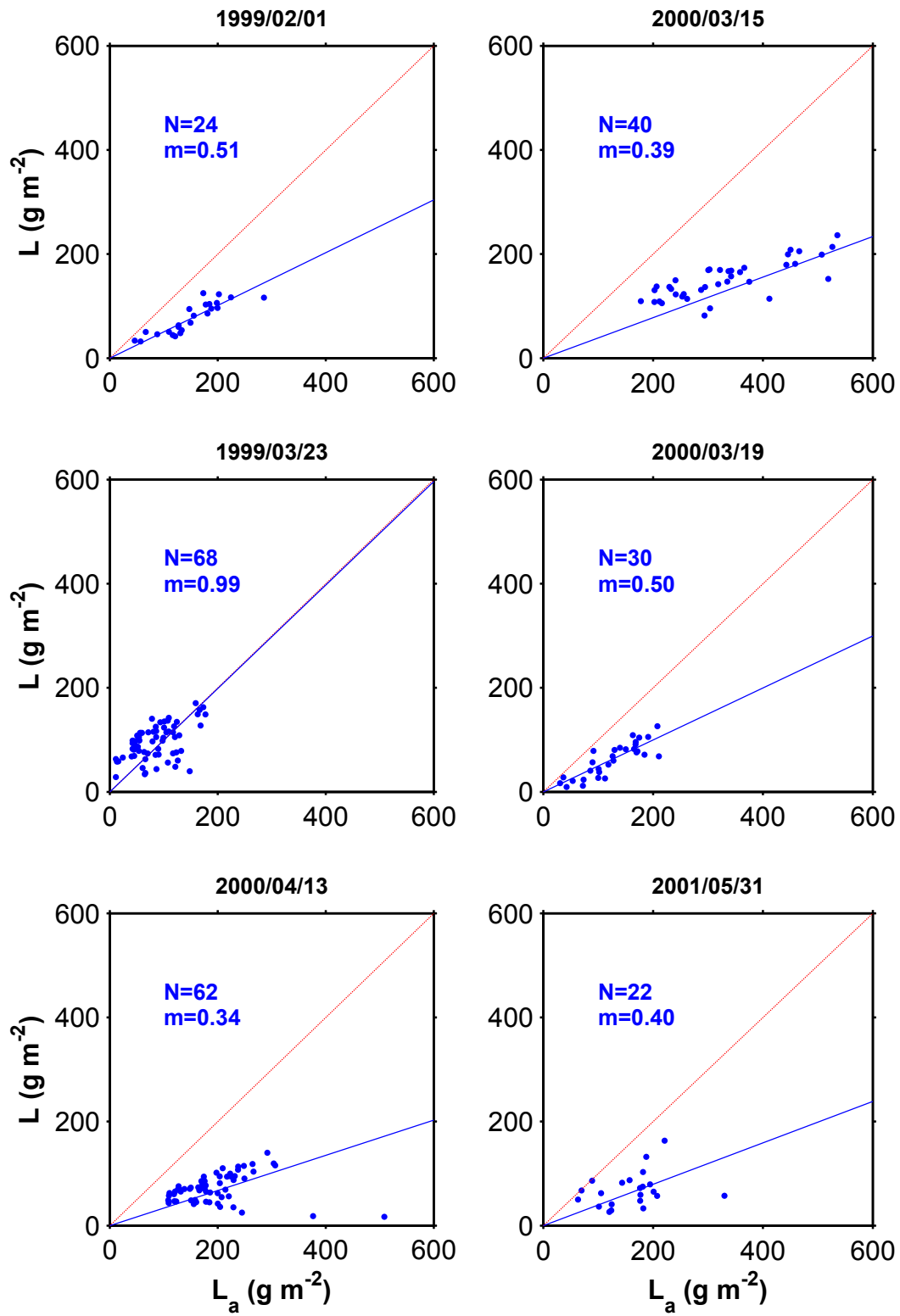


Fig. 1

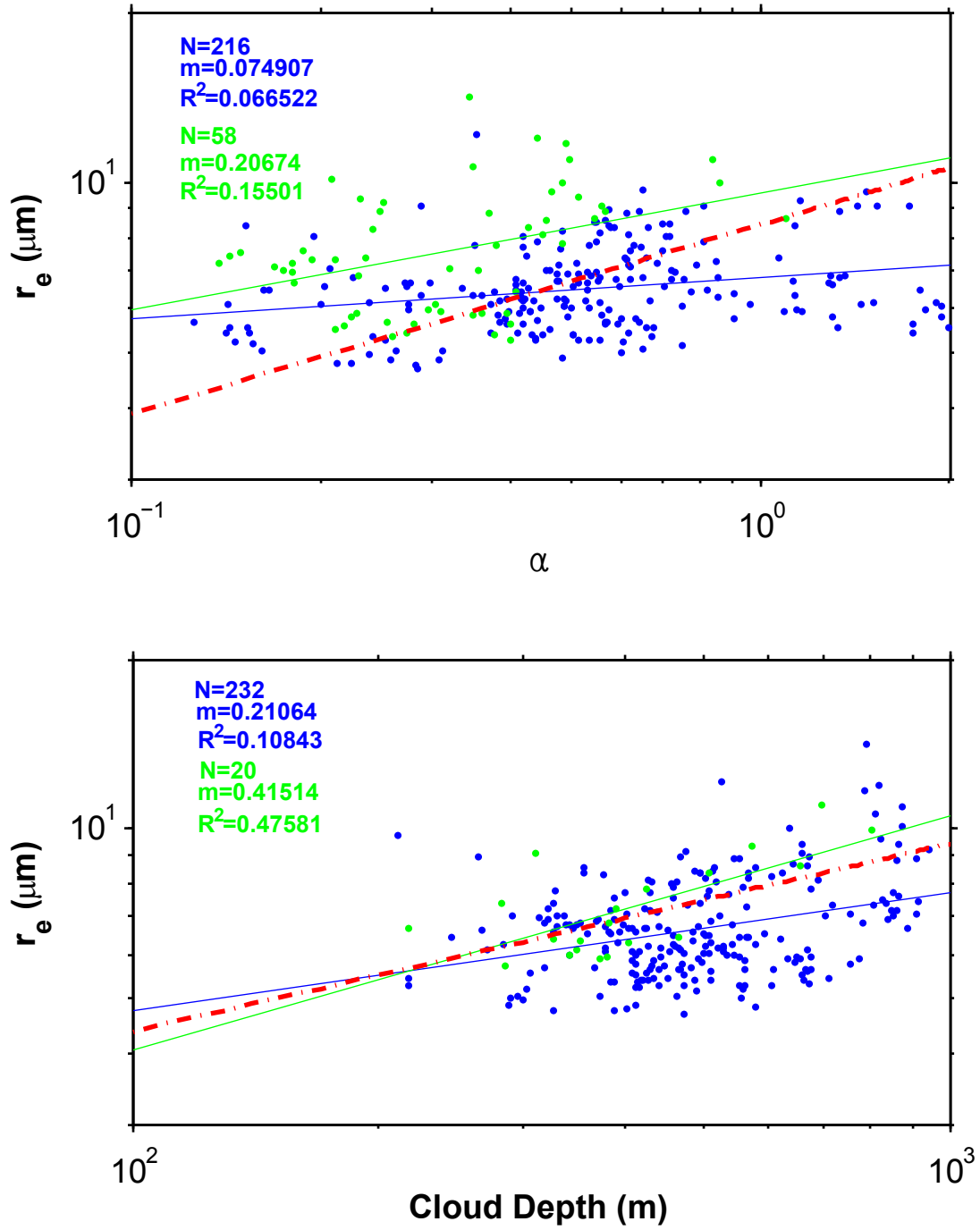


Fig. 2

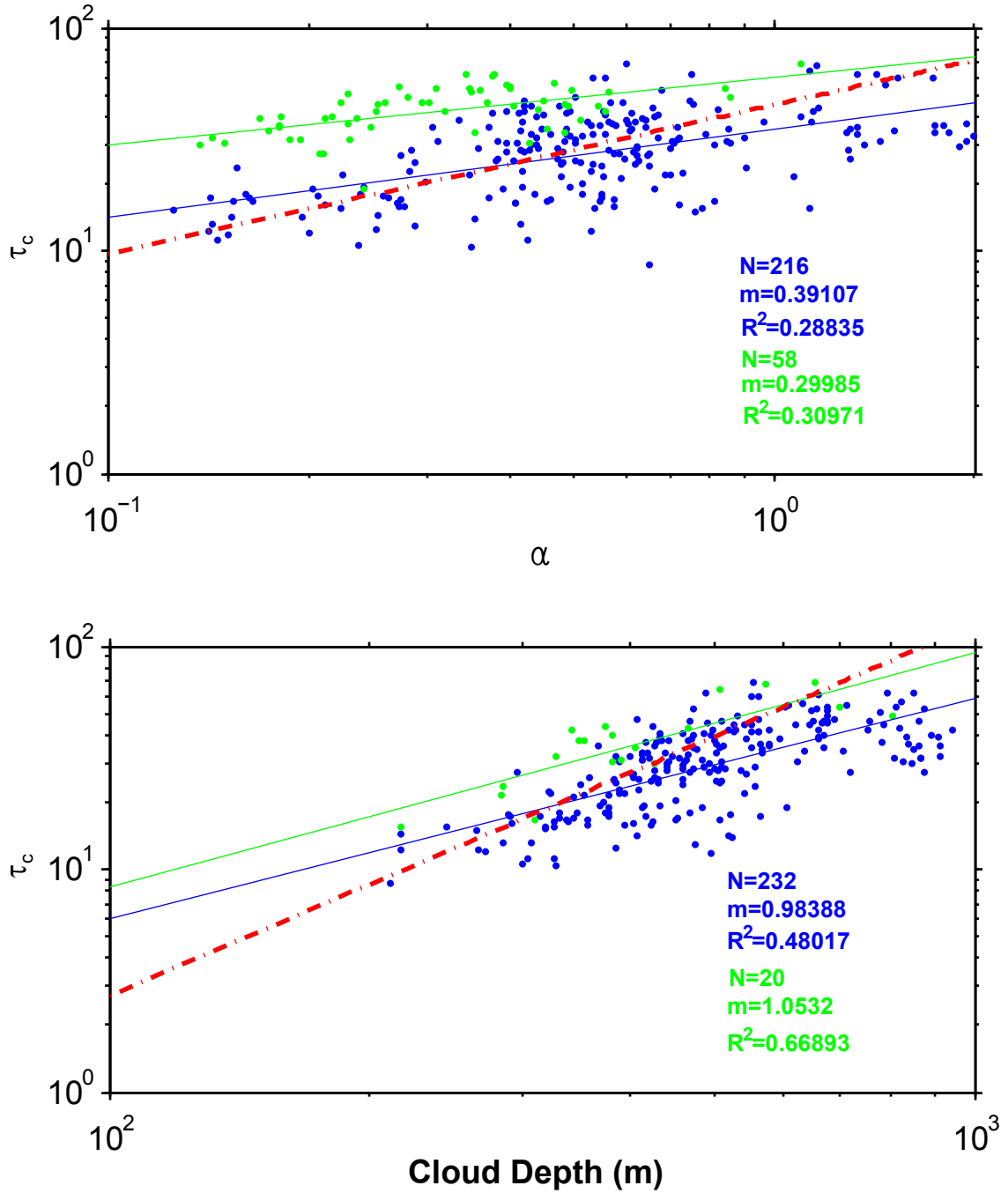


Fig. 3

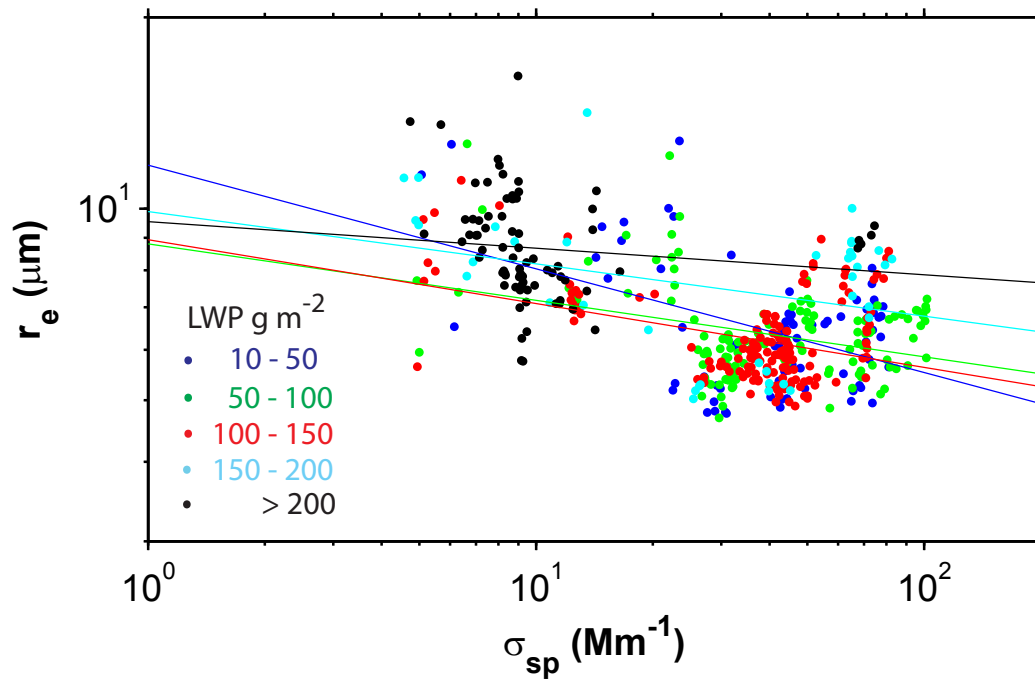
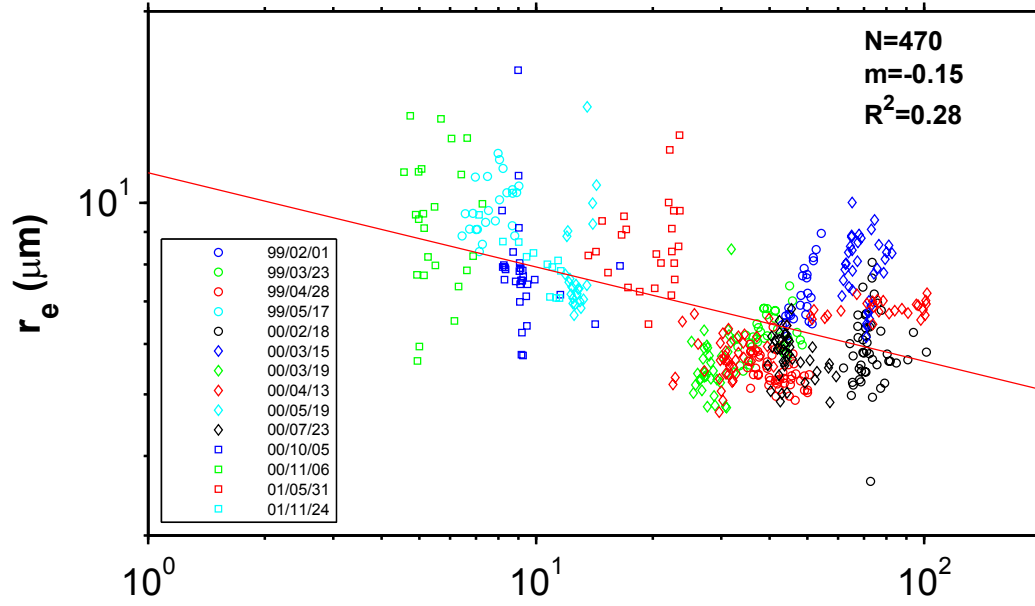


Fig. 4

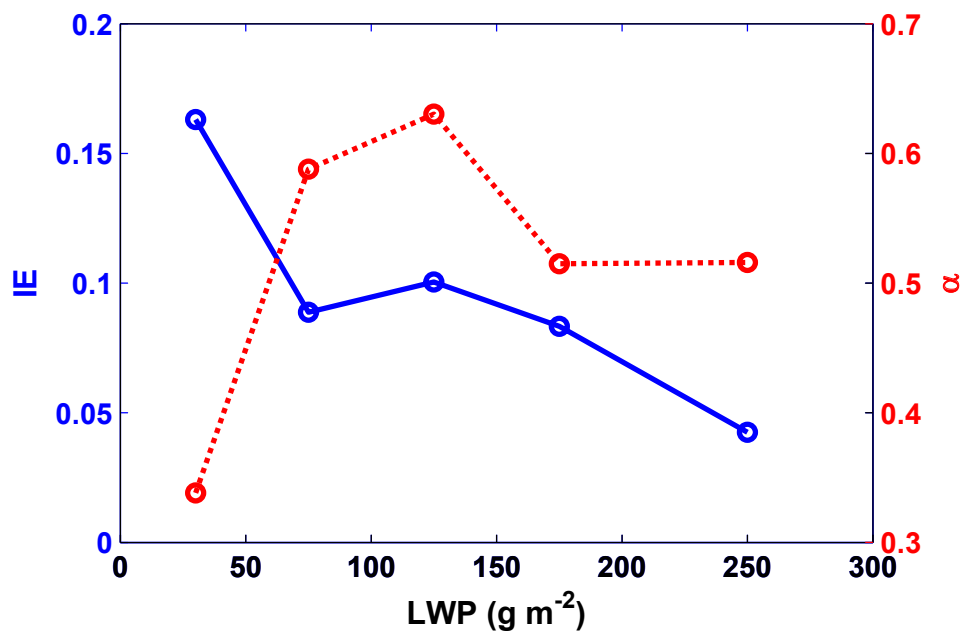


Fig. 5

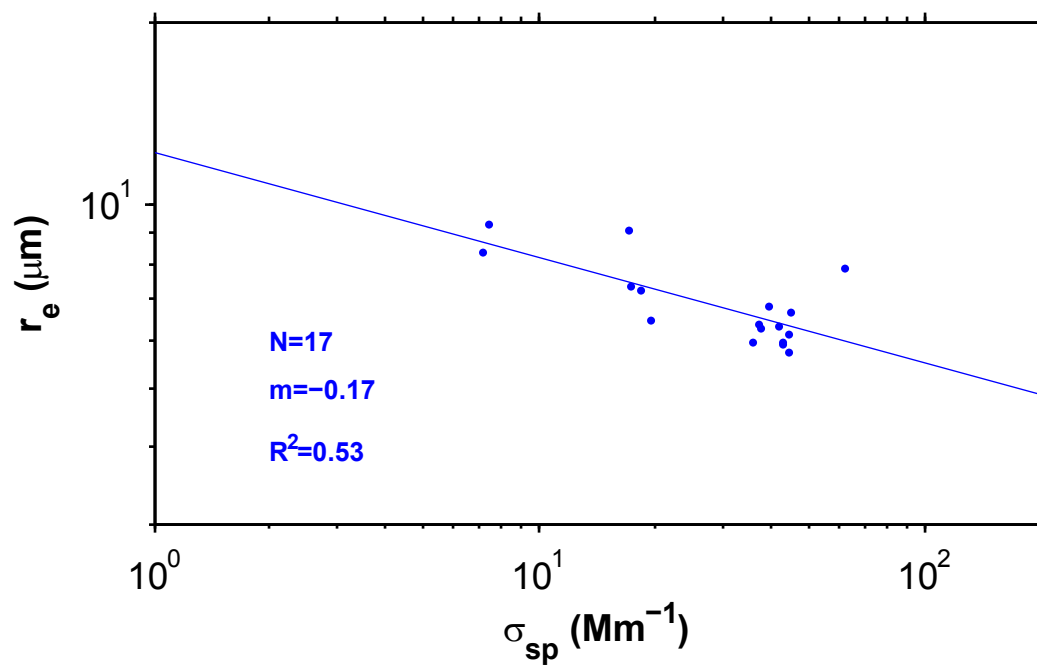
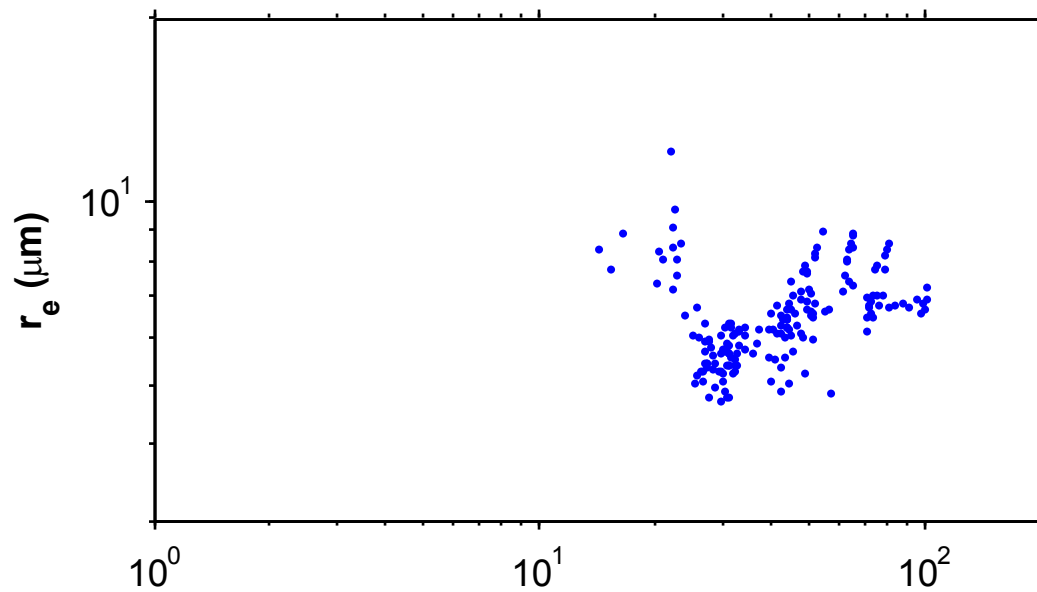


Fig. 6

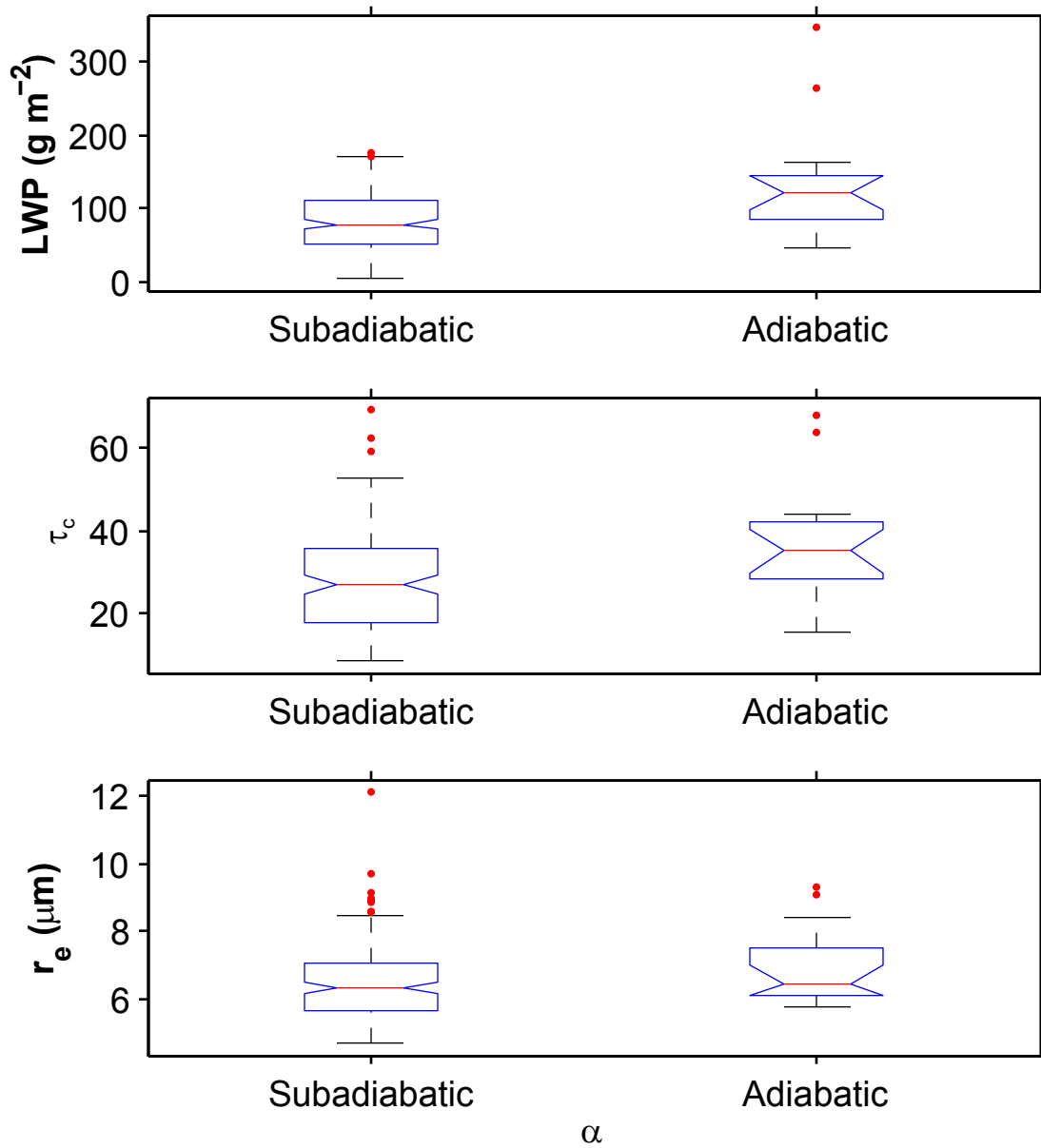


Fig. 7